PHYSICAL REVIEW D **96,** 024059 (2017)

Unstable marginally outer trapped surfaces in static spherically symmetric spacetimes

Ivan Booth[*] and Hari K. Kunduri[†]

Department of Mathematics and Statistics, Memorial University of Newfoundland, St. John's, Newfoundland and Labrador A1C 5S7, Canada

Anna O'Grady[‡]

Department of Physics and Physical Oceanography, Memorial University of Newfoundland, St. John's, Newfoundland and Labrador A1C 5S7, Canada and Dunlap Institute for Astronomy and Astrophysics Department of Astronomy and Astrophysics, University of Toronto, 50 George Street, Toronto, Ontario M5S 3H4, Canada

(Received 12 May 2017; published 31 July 2017)

We examine potential deformations of inner black hole and cosmological horizons in Reissner-Nordström de Sitter spacetimes. While the rigidity of the outer black hole horizon is guaranteed by theorem, that theorem applies to neither the inner black hole nor the past cosmological horizon. Further, for pure de Sitter spacetime, it is clear that the cosmological horizon can be deformed (by translation). For specific parameter choices, it is shown that both inner black hole and cosmological horizons can be infinitesimally deformed. However, these do not extend to finite deformations. The corresponding results for general spherically symmetric spacetimes are considered.

DOI: 10.1103/PhysRevD.96.024059

I. INTRODUCTION

In stationary spacetimes, the event horizon of a black hole is a Killing horizon and foliated by surfaces with vanishing outward null expansion: marginally outer trapped surface (MOTS). More generally, given a Cauchy surface in any spacetime, the boundary of the trapped region is an apparent horizon which is also a MOTS. Motivated by these facts, MOTS are key to many definitions of black hole boundaries including trapping horizons [1], marginally trapped tubes [2], isolated and dynamical horizons [3], the proposed core of the trapped region [4], and the very recent future holographic screens [5].

Apart from being foliated by MOTS, the event horizons of the standard stationary black hole solutions (for example, Kerr-Newman-de Sitter) have another property: they separate the trapped region from the untrapped region, and in particular, there are fully trapped surfaces uniformly close to and "just inside" the MOTS. MOTS with slight variations of this property go by many names including *stable* [6], *outer trapping* [1], or *strictly stably outermost* [7]. MOTS with one of these properties and which foliate a stationary event horizon have been shown to be geometrically rigid against deformations [7,8].

However, even in stationary spacetimes, stable horizons are the (admittedly very important) exception rather than the rule. Consider, for example, Reissner-Nordström-de Sitter as depicted in Fig. 1. Focusing on the shaded region, the inner black hole and past cosmological horizons have trapped surfaces outside rather than inside and so are not stable.[1]

Further, there is at least one case where an unstable horizon *can* be smoothly deformed. Pure de Sitter spacetime is homogeneous and isotropic with a constant positive Ricci curvature $\mathcal{R} = 4\Lambda$ determined by the cosmological constant. However, around any point p in the space, it is possible to construct the standard static coordinate patch,

$$ds^2 = -\left(1 - \frac{\Lambda}{3}r^2\right)dt^2 + \frac{dr^2}{1 - \frac{\Lambda}{3}r^2} + r^2 d\Omega^2 \qquad (1)$$

from which it is straightforward to show that there is a MOTS at

$$r_{\mathrm{CH}} = l \equiv \sqrt{\frac{3}{\Lambda}}. \qquad (2)$$

Like the cosmological horizons in Reissner-Nordström-de Sitter (RNdS), it is not stable, and it is intuitively clear that in this case, we can deform the MOTS. To see this construct, an analogous MOTS around a point p' infinitesimally close to p. This represents a deformation of the p-MOTS which in this case is essentially a translation.

[*]ibooth@mun.ca
[†]hkkunduri@mun.ca
[‡]ogrady@astro.utoronto.ca

[1]The terminology of outside versus inside becomes ambiguous in some of these cases but we will return to clarify this in Sec. II B.

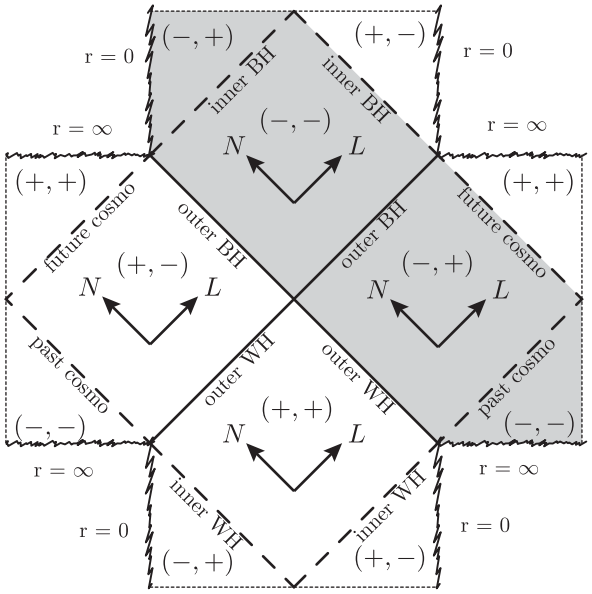

FIG. 1. One tile of the Penrose-Carter diagram for Reissner-Nordström-de Sitter spacetime. It repeats (subject to possible identifications) across the dotted lines. The various Killing horizons are labeled: outer and inner black hole, outer and inner white hole, and future and past cosmological horizons. The null directions are consistently labeled as L and N with the signs of $\theta_{(L)}$ and $\theta_{(N)}$ in each region being, respectively, listed as $(\pm,\pm)$. $\theta_{(L)}$ and $\theta_{(N)}$ vanish on the horizons to which they are tangent. Stable horizons are solid lines while unstable are dashed. Most of our discussion will focus on the shaded region containing outer and inner black hole horizons along with the past-cosmological horizon.

So at least in this case, the lack of stability corresponds to a freedom to deform the MOTS. In the rest of this paper, we will explore unstable MOTS in more detail. Section II reviews basic nomenclature and geometry along with the standard stability result. Section III shows that only particular finely tuned unstable MOTS in RNdS can be infinitesimally deformed. Section IV examines whether these infinitesimal deformations can be made finite (and so real). Section V summarizes and discusses our results. Appendix reviews some useful identities for Legendre polynomials that are applied in the main text.

II. BACKGROUND AND GENERAL THEORY

We begin with a very brief review of the mathematics and geometry of marginally outer trapped surfaces and their deformations. As general references for the next two subsections, see [8] for more details on the geometry or [9] for a review of the various types MOTS and their complications.

A. Spacetime and two-surface geometry

Let (M, g_{ab}, ∇_a) be a $(3+1)$-dimensional time-oriented spacetime and $(S, \tilde{q}_{ab}, d_a)$ be a spacelike closed and orientable two-surface embedded in M.

The normal space at each $p \in S$ is two dimensional and timelike and so can be spanned by a pair of null vectors. In particular, since M is time oriented, we may define a pair of future-oriented vector fields ℓ and n over S which do this job in each normal space. Since they are null vector fields, they each have 1 degree of rescaling freedom. However, one of these is removed by requiring that they be cross scaled so that $\ell \cdot n = -1$.

Geometric consistency requires that the combined induced metric/projection operator on S satisfies

$$\tilde{q}_{ab} = g_{ab} + \ell_a n_b + n_a \ell_b. \tag{3}$$

This fixes the intrinsic geometry of S while the extrinsic geometry comes from tangential derivatives of the null normals. These are the connection on the normal bundle

$$\tilde{\omega}_a = -\tilde{q}^c_a n_b \nabla_c \ell^b, \tag{4}$$

and the extrinsic curvatures

$$k^{(\ell)}_{ab} = \tilde{q}^c_a \tilde{q}^d_b \nabla_c \ell_d \quad \text{and} \quad k^{(n)}_{ab} = \tilde{q}^c_a \tilde{q}^d_b \nabla_c n_d, \tag{5}$$

which may be conveniently decomposed into their trace and trace-free parts

$$k^{(\ell)}_{ab} = \frac{1}{2}\theta_{(\ell)} \tilde{q}_{ab} + \sigma^{(\ell)}_{ab} \quad \text{and} \quad k^{(n)}_{ab} = \frac{1}{2}\theta_{(n)} \tilde{q}_{ab} + \sigma^{(n)}_{ab}. \tag{6}$$

Respectively, these are the expansions and the shears of those vector fields. The reason for these names is clear if we consider their alternate definition as deformations (also known as variations [7]).

Consider a vector field X^a, which is normal to S and defined in a neighborhood of the surface. Hence, on S,

$$X^a = A\ell^a - Bn^a \tag{7}$$

for some functions A and B.[2] Then that function defines a flow which can be used to evolve and deform S.

In coordinate terms, if $x^\alpha_S(\theta, \phi)$ is a (local) parametrization of S then infinitesimally the deformation sends

$$x^\alpha_S(\theta, \phi) \to x^\alpha_S(\theta, \phi) + \varepsilon X^\alpha(\theta, \phi). \tag{8}$$

The evolution also identifies points on the original and deformed surfaces along the lines of flow. Thus, one may consider the rate of change of the geometric properties of the surface under the deformation, and we denote this

[2]The negative sign for B is a convention chosen in [8] to simplify calculations when studying dynamical horizons. Even though they are not considered here, we retain the sign for consistency with that paper from which we draw almost all of our formulas.

differential operator as δ_X. It is usually referred to as either the *deformation operator* or *variation* with respect to X.

If the coordinate system is adapted to S and X^a so that S is a level surface and $X = \partial/\partial\lambda$ a coordinate vector field then δ_X, the Lie derivative $\mathcal{L}_X$, and the partial derivative $\partial/\partial\lambda$ are all the same thing. This equivalence is often used to simplify discussions of deformations in spherical symmetry. See, for example, [1].

It is not hard to show that

$$\delta_X \tilde{q}_{ab} = A k^{(\ell)}_{ab} - B k^{(n)}_{ab}, \tag{9}$$

whence

$$\delta_X \tilde{\epsilon}_{ab} = (A\theta_{(\ell)} - B\theta_{(n)})\tilde{\epsilon}_{ab}, \tag{10}$$

where $\tilde{\epsilon}$ is the area two form on S (in coordinate form $\tilde{\epsilon} = \sqrt{\tilde{q}} d\theta \wedge d\phi$). Thus, $\theta_{(X)}$ and $\sigma^{(X)}_{CD}$ are, respectively, the expansion and shear of S as it is evolved by X^a. Note too that for these intrinsic quantities, the rates of change are independent of how X^a extends off S.

One can also calculate variations of the extrinsic quantities; however, for our purposes, we only need

$$\begin{aligned}\delta_X \theta_{(\ell)} = {} & \kappa_X \theta_{(\ell)} - d^2 B + 2\tilde{\omega}^a d_a B - B(-d_a\tilde{\omega}^a + \|\tilde{\omega}\|^2 \\ & - \tilde{K} + G_{ab}\ell^a n^b - \theta_{(\ell)}\theta_{(n)}) \\ & + A(-\|\sigma^{(\ell)}\|^2 - G_{ab}\ell^a\ell^b - (1/2)\theta^2_{(\ell)}).\end{aligned} \tag{11}$$

Newly appearing quantities are $\kappa_X = -X^a n_b \nabla_a \ell^b$, $\tilde{K}$ the Gaussian curvature of S, and G_{ab} the Einstein tensor. Further, we have abbreviated $d^2 = d^a d_a$, $\|\tilde{\omega}\|^2 = \tilde{\omega}^a\tilde{\omega}_a$ and $\|\sigma^{(\ell)}\|^2 = \sigma^{(\ell)ab}\sigma^{(\ell)}_{ab}$.

Unlike (9), this variation does depend on derivatives off S. This is through the gauge dependent κ_X term which under rescalings $\ell \to e^f \ell$ and $n \to e^{-f} n$ of the null vectors transforms as

$$\kappa_X \to \kappa_X - \mathcal{L}_X f. \tag{12}$$

However, as will now be seen, we are only really interested in situations where $\theta_{(\ell)}$ vanishes and so do not need to worry about this dependence.

B. MOTS: Definition, deformation, and difficulties

The standard classification of two dimensional surface as trapped, untrapped, or marginally trapped assumes that one can unambiguously assign one of the null directions (say ℓ) as outward pointing and the other (n) as inward pointing. Then a closed, spacelike two dimensional surface S is *outer untrapped* if $\theta_{(\ell)} > 0$, an *outer trapped* if $\theta_{(\ell)} < 0$, and *marginally outer trapped (MOTS)* if $\theta_{(\ell)} = 0$. A fully *trapped* surface has both $\theta_{(\ell)} < 0$ and $\theta_{(n)} < 0$.

A Killing horizon is null, and so if it is tangent to the outgoing direction ℓ, then any two-dimensional slice of that horizon is a MOTS. Thus, for those MOTS

$$\delta_\ell \theta_{(\ell)} = -\|\sigma^{(\ell)}\|^2 - G_{ab}\ell^a\ell^b = 0. \tag{13}$$

Now, intuitively, the outer black hole Killing horizon of a stationary spacetime should have outer trapped surfaces "just inside". In terms of deformations, the existence of such surfaces implies that for some inward-oriented spacelike normal vector field $R = \alpha\ell - \beta n$ ($\alpha\beta < 0$),

$$\delta_R \theta_{(\ell)} = -d^2\beta + 2\tilde{\omega}^a d_a\beta - \beta\delta_n\theta_{(\ell)} < 0, \tag{14}$$

where

$$\delta_n \theta_{(\ell)} = -d_a\tilde{\omega}^a + \|\tilde{\omega}\|^2 - \tilde{K} + G_{ab}\ell^a n^b. \tag{15}$$

The vanishing of $\delta_\ell\theta_{(\ell)}$ renders the value of α irrelevant. Note too that if we rescale the null vectors so that $n \to \beta n$ (and $\ell \to \ell/\beta$), this condition becomes $\delta_n\theta_{(\ell)} < 0$.[3]

Now, a closed MOTS slice S of a Killing horizon with $\delta_n\theta_{(\ell)} < 0$ is guaranteed to be geometrically stable in that it cannot be smoothly deformed out of the Killing horizon while preserving $\theta_{(\ell)} = 0$. To see this, consider variations generated by a vector field X of the form (7) with B not everywhere vanishing (that would correspond to a variation along the Killing horizon). Then any such MOTS-preserving variation of S necessarily satisfies

$$\delta_X \theta_{(\ell)} = 0. \tag{16}$$

However, as considered above $\delta_\ell\theta_{(\ell)} = 0$ and again A is irrelevant. Thus, the variation must satisfy

$$-d^2 B + 2\tilde{\omega}^a d_a B - B\delta_n\theta_{(\ell)} = 0. \tag{17}$$

For $\delta_n\theta_{(\ell)} < 0$, there are no solutions to this equation and so no MOTS-preserving variation [7] (this can also be seen by a maximum principle argument [8]).

MOTS satisfying versions of this condition have been considered many times over the years, and among other names have been termed *stable* [6], *outer trapping* [1], or *strictly stably outermost* [7]. In this paper, we will generally refer to them as stable.

This setup and labeling is all very well for outer black hole horizons in a spacetime with an unambiguous notion of ingoing and outgoing; however, in a multihorizon spacetime like that shown in Fig. 1, outward and inward labels are not well-defined. Neither L nor N is consistently

[3]Restricting attention spherical horizons, the correct scaling is obvious but for a concrete demonstration of a less trivial situation, see the discussion of Kerr in Appendix C of [8].

outward pointing (towards an $r = \infty$) or inward pointing (towards an $r = 0$).

While there are systems of nomenclature that distinguish between the various types of horizons without reference to "inner" and "outer" [10,11], for this paper, we will instead just abuse the name "MOTS" and use it to refer to any surface with one vanishing null expansion. We will always label that direction ℓ (so that $\theta_{(\ell)} = 0$) and the other future null direction n. Note that the geometric stability arguments made in the paragraph surrounding (17) continue to apply regardless of the orientation of ℓ and n. Thus, we may always test the geometric stability of a MOTS by checking for a scaling of the null vectors such that $\delta_n\theta_{(\ell)} < 0$.

Turning once again to Fig. 1, we see that on some horizons $\ell = L$ while on others we will have $\ell = N$. However, whatever the labeling, the outer black and white hole horizons are stable by this measure while all cosmological and inner black hole horizons are potentially unstable with $\delta_n\theta_{(\ell)} > 0$.

For the rest of this paper, we will investigate whether this potential instability translates into finite MOTS-preserving variations.

III. "UNSTABLE" MOTS IN RNDS

In the last section, we tested stability based on how the null expansions do or do not change signs across a horizon. However, to understand whether the lack of a proof of stability actually corresponds to a real instability, we need more calculations and commence with finding exact expressions for $\delta_n\theta_{(\ell)}$.

First, the RNdS metric in standard form [static for $F(r) > 0$] is

$$ds^2 = -F(r)dt^2 + \frac{dr^2}{F(r)} dr^2 + r^2 d\Omega^2 \tag{18}$$

with

$$F(r) = -\frac{\Lambda}{3} r^2 + 1 - \frac{2m}{r} + \frac{q^2}{r^2}. \tag{19}$$

The horizons are located at roots of $F(r)$. For black hole solutions like that depicted in Fig. 2, there is one negative, unphysical, root and three positive roots that correspond to horizons. In increasing order, these are the inner black/white hole horizons at r_{IH}, outer black/white hole horizons r_{OH}, and future and past cosmological horizons r_{CH}. However, not all members of this family of solutions are cosmological black holes. Figure 3 shows the allowed parameter range. It was produced by examining where the discriminant of F vanishes (these are double or triple roots and so the boundaries of the "regular" region).

For spherically symmetric $r =$ constant surfaces and a similarly symmetric scaling of the null vectors, we have $\tilde{\omega}_a = 0$. Thus, (15) becomes

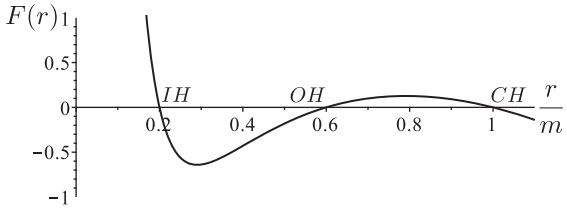

FIG. 2. $F(r)$ for a typical cosmological black hole solution. In this case, $\Lambda \approx 0.1417/m^2$ and $q^2 \approx 0.8496m^2$. The inner black hole horizon, outer black hole horizon, and cosmological horizon are respectively labeled as IH, OH, and CH.

$$\delta_n\theta_{(\ell)}|_{\mathrm{spherical}} = -\frac{1}{r^2} + G_{ab}\ell^a n^b. \tag{20}$$

Note that this is invariant with respect to the scaling of the null vectors, and in fact, we can find it without ever defining them. By (3), $G_{ab}\ell^a n^b = \frac{1}{2}G_{ab}(\tilde{q}^{ab} - g^{ab})$ so

$$\delta_n\theta_{(\ell)}|_{\mathrm{RNdS}} = -\frac{F'}{r}, \tag{21}$$

where the prime indicates a derivative with respect to r, and we have applied $F(r) = 0$. With $\Lambda > 0$, the asymptotic behavior is fixed and so the requirement that there be three positive roots means that $F(r)$ will generically take a form similar to Fig. 2. In particular, it is clear that

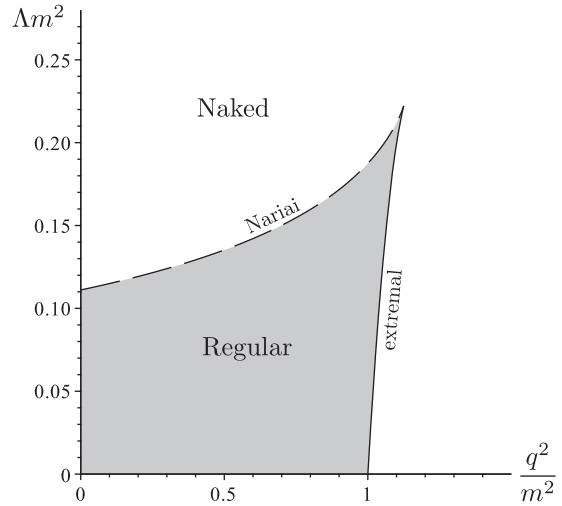

FIG. 3. Phase space of RNdS spacetimes with $m \neq 0$. Λ and q^2 are given in units of m. Solutions with three horizons (inner black hole, outer black hole, cosmological) are found in the grey shaded region while naked solutions with a single cosmological horizon form the rest of the phase space. The only exception is pure RN along the $\Lambda = 0$ line, where for $q < m$ there are inner and outer black hole horizons while $q > m$ is horizon free. Along the dashed line outer and cosmological horizons are degenerate as in the Nariai limit of SdS while the solid line represents extremal black holes. Where the lines meet, all three horizons are degenerate.

$$\delta_n\theta_{(\ell)}|_{\rm OH} < 0 \quad \text{while } \delta_n\theta_{(\ell)}|_{\rm IH,CH} > 0 \tag{22}$$

as claimed earlier.

However, we now demonstrate that in (at least) the vast majority of cases the inner and cosmological horizons are also stable. To see this, we consider concrete solutions of the stability equation (17). On both horizons, this becomes

$$\nabla^2 B + (r^2\delta_n\theta_{(\ell)})B = 0, \tag{23}$$

where $\nabla^2 B$ is the regular spherical Laplace operator on a unit sphere. Thus, potential deformations must satisfy

$$\nabla^2 B = (rF')B. \tag{24}$$

The only nondiverging solutions of the spherical Laplace eigenvalue equation are spherical harmonics. That is if there is an integer l such that

$$-rF' = l(l+1) \tag{25}$$

then (24) has solutions

$$B = P_l(\cos\theta)(A_m\cos(m\phi) + B_m\sin(m\phi)) \tag{26}$$

for integers $0 \le m < l$ and constants A_m and B_m.

We can then test for cases where these conditions might be met. First, for $m = 0$, the only non-naked singularity spacetime is pure de Sitter. In that case, it is straightforward to see that $-rF' = 2$ on the cosmological horizon and so the MOTS-translation freedom manifests itself as an $l = 1$ instability.

Turning to $m \neq 0$, Fig. 4 shows the values $-rF'$ for all horizons in RNdS black hole spacetimes, and so we can consider them case by case.

First, for the outer horizon, $-1 \le -rF' \le 0$, and so there are no possible solutions. This is not a surprise as we have already twice concluded that outer black and white hole horizons are stable.

Similarly simple is the inner horizon with $0 \le -rF' < \infty$. In this case, a correct choice of parameter values will allow any possible l. In particular, this is even possible for pure RN.

The cosmological horizon is a little more subtle. The figure shows that the only possible case is $-rF' = 2 \Leftrightarrow l = 1$; however, this limit is not achieved: it is along the $\Lambda = 0$ line, where there is not a cosmological horizon. So for $m \neq 0$, there are no solutions and the cosmological horizon is stable.

Thus, we have now explicitly demonstrated that while the stability condition $\delta_X\theta_{(\ell)} < 0$ may be sufficient to exclude deformations, it certainly is not necessary. Examples are the cosmological horizon in $m \neq 0$ RNdS spacetimes and (at least) all but a finely tuned set of inner horizons. In the next section, we will further examine those special cases.

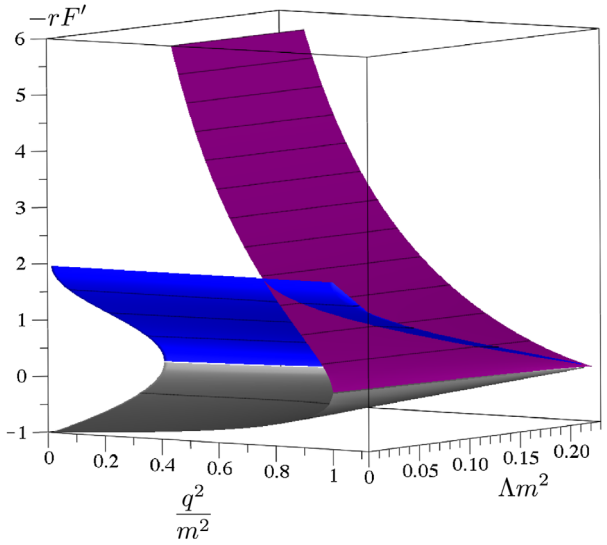

FIG. 4. Values of $r^2\delta_n\theta_{(\ell)} = -rF'$ for cosmological (blue), outer (grey), and inner (purple) horizons. Potential instabilities exist when $-r\frac{dF}{dr} = l(l+1)$ for some positive integer l. Though it is cut off in the figure, the inner horizon sheet diverges to infinity. The domain for all horizons is as shown in Fig. 3.

IV. FINITE DEFORMATIONS IN RNDS

In this section, we develop the formalism necessary to test the higher order stability of the special cases that were found to be first order unstable in the previous section. It is easiest to do this by moving away from the general formalism of Sec. II and to one specialized to the RNdS spacetimes. In all the cases that we check, we will see that the apparent first-order instability fails at higher order.

A. MOTS in Painlevé-Gullstrand coordinates

We begin by introducing Painlevé-Gullstrand (PG) coordinates for RNdS spacetimes. Recall that time in these coordinates is measured along a congruence of infalling timelike geodesics while the spatial slices of constant time are intrinsically flat [12]. For RNdS, the shaded patch shown in Fig. 1 is (almost) covered by coordinates (T, r, θ, ϕ) with metric,

$$ds^2 = -F(r)dT^2 + 2\sqrt{1-F(r)}dTdr + dr^2 + r^2d\Omega^2, \tag{27}$$

where $F(r)$ takes its usual form (19). The "almost" is included in the previous sentence because for $q \neq 0$, there will always be a region where $1 - F < 0$ and so the coordinate system is not well-defined. However, as we shall see, for example, in Fig. 5, this will always be inside the inner horizon and so not cause us any problems.

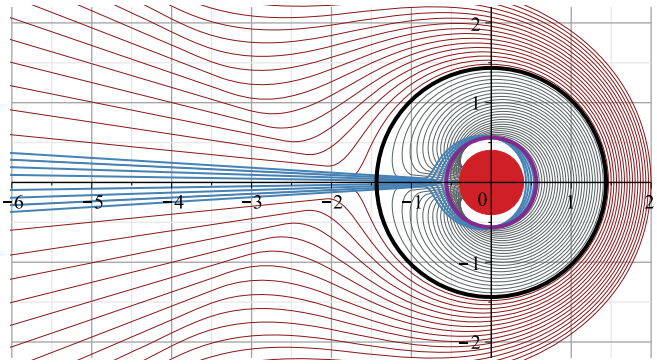

FIG. 5. Axisymmetric $\theta_{(\ell)} = 0$ surfaces in a $q/m = 0.9$ Reissner-Nordström spacetime. The inner horizon is purple and the outer horizon is black. Other (open) $\theta_{(\ell)} = 0$ surfaces are numerically solved from initial conditions (42) and (43) and colored blue, grey, or dark red depending on the value of R_o. The red circle in the middle is the region that is not covered by the PG coordinates. The z axis is horizontal with the north pole on the right-hand side.

We will look for MOTS on hypersurfaces Σ_T of constant T, and in order to do this, it will be sufficient to know the intrinsic and extrinsic geometry of Σ_T. The intrinsic geometry on Σ_T is given by the Euclidean metric,

$$d\Sigma^2 = h_{ab}dx^a dx^b = dr^2 + r^2 d\Omega^2, \tag{28}$$

while the extrinsic curvature is

$$K = \left(\frac{F'}{2\sqrt{1-F}}\right)dr^2 - (r\sqrt{1-F})d\Omega^2, \tag{29}$$

which was calculated from the future-oriented unit timelike normal to Σ_T,

$$\hat{u} = \left(\frac{\partial}{\partial T}\right) - \sqrt{1-F}\left(\frac{\partial}{\partial r}\right). \tag{30}$$

Then consider a rotationally symmetric surface S in a Σ_T and parametrize it by coordinates (λ, ϕ) as

$$(T, R, \theta, \phi) = (T_o, R(\lambda), \Theta(\lambda), \phi), \tag{31}$$

for some functions $R(\lambda)$ and $\Theta(\lambda)$. For now, we will find it convenient to take λ to be the arclength parameter as measured from the north pole of S along the constant ϕ lines of longitude. Then the tangent vector

$$\frac{d}{d\lambda} = \dot{R}\left(\frac{\partial}{\partial r}\right) + \dot{\Theta}\left(\frac{\partial}{\partial \theta}\right) \tag{32}$$

is unit length

$$\dot{R}^2 + R^2\dot{\Theta}^2 = 1, \tag{33}$$

where we have marked derivatives with respect to λ with dots.

Next the induced two metric on S is

$$dS^2 = d\lambda^2 + (R^2\sin^2\Theta)d\phi^2, \tag{34}$$

with inverse,

$$\tilde{q} = \left(\frac{\partial}{\partial\lambda}\right)\otimes\left(\frac{\partial}{\partial\lambda}\right) + \frac{1}{R^2\sin^2\Theta}\left(\frac{\partial}{\partial\phi}\right)\otimes\left(\frac{\partial}{\partial\phi}\right).$$

The positive-r pointing spacelike normal to S in Σ_T is

$$\hat{r} = R\left(\dot{\Theta}\left(\frac{\partial}{\partial r}\right) - \frac{\dot{R}}{r^2}\left(\frac{\partial}{\partial\theta}\right)\right), \tag{35}$$

whence the trace of the extrinsic curvature of S in Σ_T is

$$\theta_{(\hat{r})} \equiv \tilde{q}^{ab}\nabla_a\hat{r}_b = -\frac{\ddot{R}}{R\dot{\Theta}} + 2\dot{\Theta} - \frac{\dot{R}}{R}\cot(\Theta), \tag{36}$$

where we have used the arclength condition to somewhat simplify the expression. Note that no F appears in this expression: Σ_T is Euclidean so any geometric calculation intrinsic to Σ_T is independent of F.

Next, the trace of the extrinsic curvature of S with respect to $\hat{u}$ (and so out of Σ_T) is

$$\theta_{(\hat{u})} \equiv \tilde{q}^{ab}\nabla_a\hat{u}_b = K_{ab}h^{ab} - K_{ab}\hat{r}^a\hat{r}^b. \tag{37}$$

That is

$$\theta_{(\hat{u})} = \frac{(RF' + 2(1-F))\dot{R}^2 - 4(1-F)}{2R\sqrt{1-F}}. \tag{38}$$

Then an outward oriented null vector is $\ell = \hat{u} + \hat{r}$ and if

$$\theta_{(\ell)} = \theta_{\hat{u}} + \theta_{\hat{r}} = 0, \tag{39}$$

we can combine this with the arclength constraint (33) to get a pair of differential equations for R and Θ describing a rotationally symmetric MOTS,

$$\ddot{R} = \frac{2(1-\dot{R}^2)}{R} - \frac{\dot{R}\sqrt{1-\dot{R}^2}}{R}\cot\Theta + \frac{1}{2R}\sqrt{\frac{1-\dot{R}^2}{1-F}}((RF' + 2(1-F))\dot{R}^2 - 4(1-F)) \tag{40}$$

and

$$\dot{\Theta} = \frac{2\pi\sqrt{1-\dot{R}^2}}{R}, \tag{41}$$

where we have assumed that $\dot{\Theta} > 0$ (which turns out to be true for all the situations in which we are interested).

We need initial conditions in order to solve these equations. By the assumed symmetry, if we choose $\lambda = 0$ at $\theta = 0$ (the north pole) then

$$\dot{R}(0) = 0. \tag{42}$$

Thus, given a choice

$$R(0) = R_o \tag{43}$$

for some constant R_o, we can find a MOTS candidate. These equations can always be integrated and so by construction will always produce a $\theta_{(\ell)} = 0$ surface. Its closure or lack thereof will determine whether or not it is a MOTS. This shooting method is commonly used for finding axisymmetric apparent horizons in numerical relativity [13,14].

B. Numerical examples

Some sample $\theta_{(\ell)} = 0$ surfaces are shown in Figs. 5 and 6, which, respectively, show typical Reissner-Nordström and Schwazschild-de Sitter spacetimes. Those figures show the system (40)–(41) solved with initial conditions (42) and (43). Solutions were obtained using Maple's [15] built-in routines for systems of differential equations. Note that while the known horizons certainly show up as solutions, there is also a $\theta_{(\ell)} = 0$ surface running through all points on the positive z axis. The behaviors shown in the figures appear to be generic. Axisymmetric $\theta_{(\ell)} = 0$ surfaces that originate from $0 < R_o < r_{\rm IH}$ and $r_{\rm OH} < R_o < r_{\rm CH}$ ultimately diverge to infinity while those from $r_{\rm IH} < R_o < r_{\rm OH}$ and $r_{\rm CH} < R_o < \infty$ turn in and disappear into the singularity (or in the case with $q \neq 0$, the region where the coordinate system is no longer defined). Thus, those surfaces are not MOTS as they are not smooth and closed.

These divergences can be contrasted with the now familiar pure de Sitter case. For that spacetime

$$\theta_{\hat{u}} = -2\sqrt{\frac{3}{\Lambda}} \tag{44}$$

and so in a $T =$ constant surface, any sphere of radius

$$r_S = \sqrt{\frac{3}{\Lambda}} \tag{45}$$

will have $\theta_{(\ell)} = 0$. Examples are shown in Fig. 5 (which despite the preceding analysis were numerically evolved in the same way as the previous examples).

Note that the open $\theta_{(\ell)} = 0$ surfaces shown in Fig. 5 are not leaves of an isolated horizon [3]. That is, if a particular

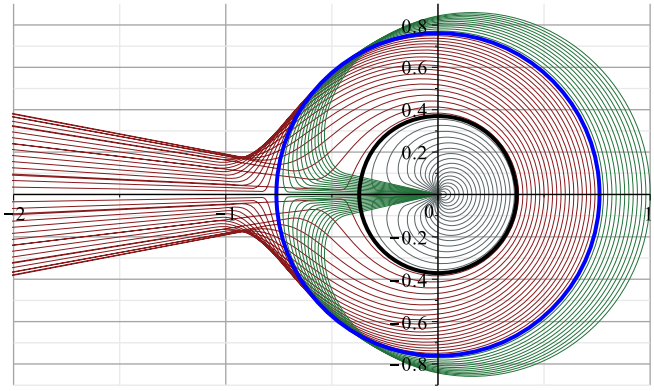

FIG. 6. Axisymmetric $\theta_{(\ell)} = 0$ surfaces in $\Lambda = 0.0768/m^2$ Schwarzschild-de Sitter spacetime. The outer black hole and cosmological horizons are, respectively, black and blue. Other (open) $\theta_{(\ell)} = 0$ surfaces are numerically solved from initial conditions (42) and (43) and grey, dark red, or green depending on the value of R_o. The z axis is horizontal with the north pole on the right-hand side.

$\theta_{(\ell)} = 0$ surface that opens up to infinity (or plunges into the singularity) is extended to a three dimensional surface as the locus of points, it traces as T varies, then that three dimensional surface is not null. So while these are $\theta_{(\ell)} = 0$ surfaces, they should not be viewed as foliating a kind of "open" horizon.

As a side note, the ubiquity of $\theta_{(\ell)} = 0$ surfaces seen in Figs. 5 and 6 serves to emphasize the nonlocal character of MOTS: finding a $\theta_{(\ell)} = 0$ surface is not difficult and in our examples, it is possible to find such a surface through any point. The hard part is finding a $\theta_{(\ell)} = 0$ that smoothly closes. Determining whether or not that happens requires an integration to find the full surface. Hence, whether or not a particular section of a $\theta_{(\ell)} = 0$ surface is part of a MOTS may be determined by the detailed geometric properties of a far-away section of spacetime.

C. Higher order stability

We now return to the first-order unstable cases found in Sec. III to investigate their stability at higher order.

We begin with numerical tests: evolving from initial conditions $R_o = r_{\rm IH} + \delta R_o$ where $r_{\rm IH}$ is the MOTS of an inner Reissner-Nordström horizon while δR_o is a finite perturbation. Finite instabilities will manifest as finite deformations (like those in Fig. 7) while higher order stability will mean that any initially finite deformation will diverge (like those in Figs. 5 and 6).

The $l = 0, 1, 2, 3$ modes are shown in Fig. 8. For $l = 0, 2$, the instability appears to fail as the numerical solutions diverge at $\theta = \pi$; however, for $l = 1, 3$, things are not so clear. In those two cases, we do not observe any divergences. However, while suggestive, these observations are not conclusive as in both cases, the behavior could change for sufficiently small δR_o.

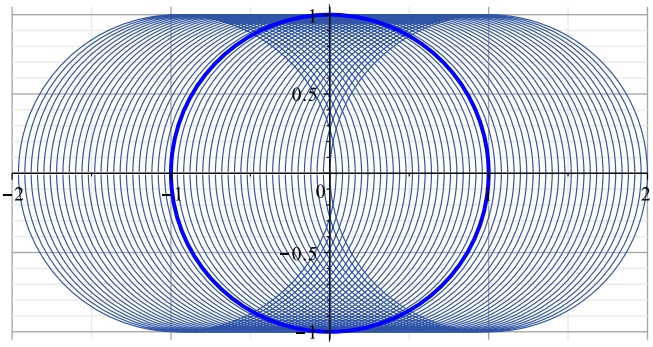

FIG. 7. Translated cosmological horizons in pure de Sitter spacetime. Coordinates are in terms of the de Sitter radius.

To better understand what is happening, we turn to a higher-order analysis of the equations. Then it is more convenient to work with a single function and so we switch to parametrize R with θ. Working from

$$\lambda_\theta = \sqrt{R_\theta^2 + R^2} \tag{46}$$

and

$$\dot{R} = \frac{R_\theta}{\lambda_\theta} \tag{47}$$

(where derivatives with respect to θ are indicated with subscripts), the conversion is straightforward, and we get the following differential equation:

$$0 = R_{\theta\theta} - \left(\frac{3}{R} + \frac{\sqrt{R^2 + R_\theta^2}}{2R^2\sqrt{1-F}}(RF' - 2(1-F))\right)R_\theta^2 + \left(\frac{R^2 + R_\theta^2}{R^2}\right)\cot\theta R_\theta - 2R + 2\sqrt{(1-F)(R^2 + R_\theta^2)}. \tag{48}$$

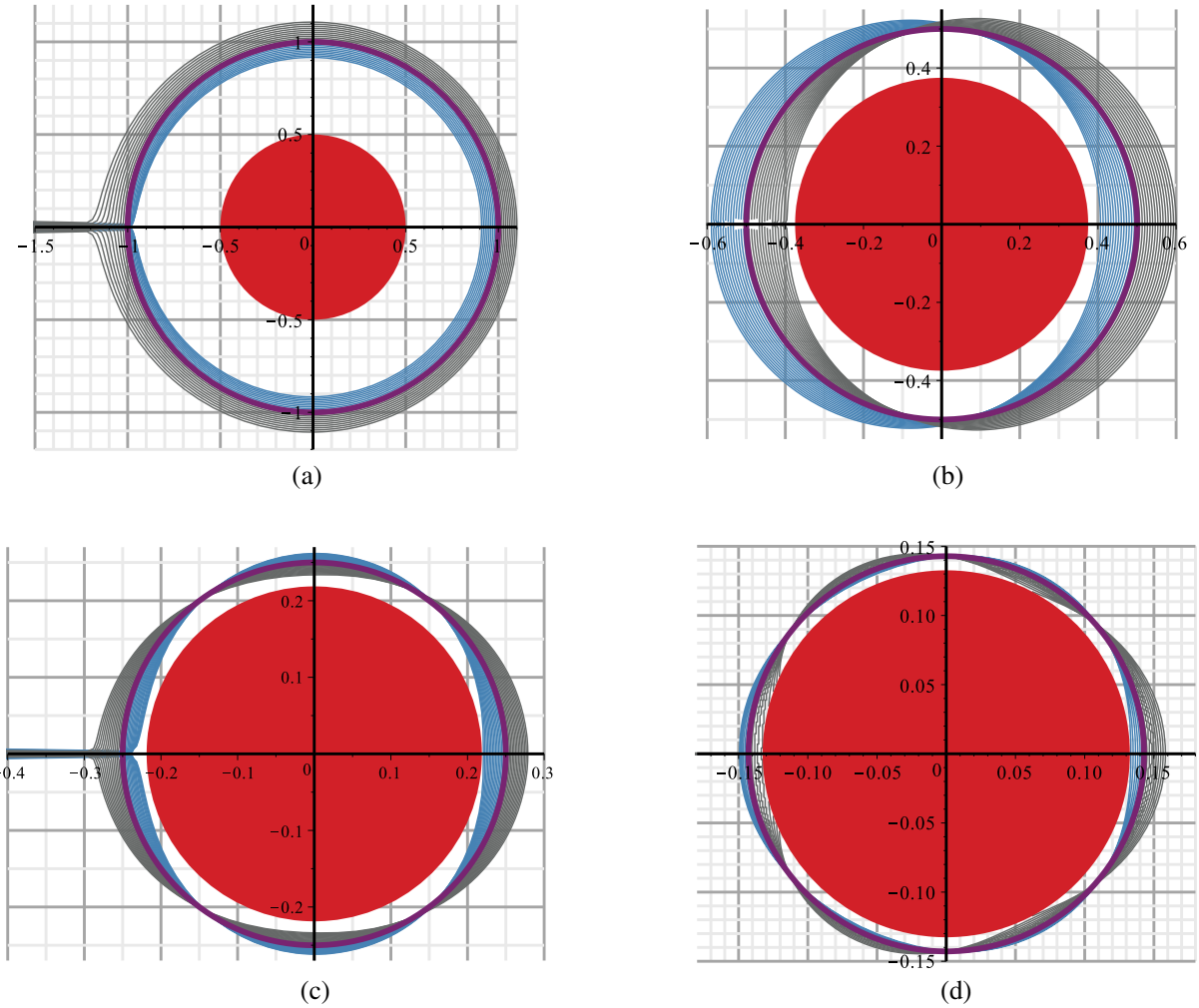

FIG. 8. Numerical solutions of first-order unstable inner Reissner-Nordström horizons for (a) $l = 0$, (b) $l = 1$, (c) $l = 2$, and (d) $l = 3$. $l = 0, 2$ appear to diverge for all sizes of initial perturbation but no divergence can be seen for $l = 1, 3$. As in Fig. 5, the red center is not covered by the PG coordinates.

Given an inner horizon at $r_{\rm IH}$ we can then look for MOTS of the form,

$$R(\theta) = r_{\rm IH} + m(\epsilon R_1(\theta) + \epsilon^2 R_2(\theta) + \epsilon^3 R_3(\theta) + \cdots), \tag{49}$$

where, of course, ϵ is the initial perturbation from $r_{\rm IH}$ at $\theta = 0$. Then, we have initial conditions

$$R_1(0) = 1 \quad \text{and} \quad R_L(0) = 0 \quad \text{for } L > 1 \tag{50}$$

while the first derivative $R_{L\theta}(0) = 0$ for all L.

We also expand $F = 1 - \frac{2m}{r} + \frac{q^2}{r^2}$ as a Taylor series around $r_{\rm IH} = m - \sqrt{m^2 - q^2}$ as

$$F(r) = \sum_{n=1}^{\infty} (-1)^n (nl(l+1) + (n-1)) \left(\frac{r - r_{\rm IH}}{r_{\rm IH}}\right)^n, \tag{51}$$

where deriving these expansion uses the first-order condition $r_{\rm IH} F_1 = -l(l+1)$.

Then to the first 3 orders (48) expands as

$$0 = \triangle_l R_1 \tag{52}$$

$$0 = \triangle_l R_2 + \left(\frac{l^2(l+1)^2 - 4}{4}\right) R_{1\theta}^2 - \left(\frac{(l^2+l+2)^3}{8}\right) R_1^2 \tag{53}$$

$$\begin{aligned} 0 = {} & \triangle_l R_3 + \left(\frac{(l^2+l+2)^2 \cot\theta}{4}\right) R_{1\theta}^3 \\ & - \left(\frac{l(l+1)(l^2+l+2)^2(l^2+l+4)}{16}\right) R_1 R_{1\theta}^2 \\ & + \left(\frac{l^2(l+1)^2 - 4}{2}\right) R_{1\theta} R_{2\theta} \\ & - \left(\frac{(l^2+l+2)^3}{4}\right) R_1 R_2 + \left(\frac{(l^2+l+2)^5}{32}\right) R_1^3, \end{aligned} \tag{54}$$

where $\triangle_l$ is the second-order differential operator that vanishes for first-order unstable perturbations (24),

$$\triangle_l = \frac{d^2}{d\theta^2} + \cot\theta \frac{d}{d\theta} + l(l+1). \tag{55}$$

In the following, we refer to the non-$\triangle_l R_n$ terms in each equation as h_{ln}.

Of course, the R_1 equation is (24) again. Note that the equations can be solved sequentially. Once we have R_1, we can solve for R_2 and then both of them can be used to solve for R_3. While the rapidly growing complexity of the expressions means that it is not practical to show the higher order equations, this pattern continues.

Then, we are interested in solutions to equations of the form

$$\triangle_l X + h(\theta) = 0, \tag{56}$$

where $X(\theta) : [0, \pi] \to \mathbb{R}$ satisfies initial conditions $X(0) = X_o \in \mathbb{R}$, $X_\theta(0) = 0$, and $h(\theta)$ can be expressed as a finite sum of Legendre polynomials,

$$h(\theta) = \sum_{L=0}^{L_{\max}} h_{[L]} P_L(\cos\theta). \tag{57}$$

Now, the solution to the homogeneous version of (56) is the Legendre polynomial $P_l(\cos\theta)$. Therefore, by the Fredholm alternative theorem, the inhomogeneous problem has a solution if and only if $h(\theta)$ is orthogonal to $P_l(\cos\theta)$,

$$h_{[l]} \equiv \frac{2l+1}{2} \int_0^\pi \sin\theta h(\theta) P_l(\cos\theta) d\theta = 0. \tag{58}$$

Equivalently, the Legendre polynomial expansion of h does not contain an h_l term.

If a solution does exist then it is also a finite sum of Legendre polynomials,

$$X(\theta) = \sum_{L=0}^{L_{\max}} X_L P_L(\cos\theta), \tag{59}$$

where for $L \neq l$

$$X_L = \frac{h_{[L]}}{L(L+1) - l(l+1)} \tag{60}$$

and

$$X_l = X_0 - \sum_{L=0}^{L_{\max}} \Big|_{L \neq l} X_L. \tag{61}$$

These observation can then be combined as an algorithm to test for solutions to the deformation problem to arbitrary order.

(1) Set $R_1 = \epsilon m P_l(\cos\theta)$ and $n = 2$.

(2) Find the ϵ^n term in the expansion of (48). It will take the form

$$\triangle_l R_n + h_{ln} = 0, \tag{62}$$

where h_{ln} will always be a sum of terms involving $l, \cot\theta, R_1, R_{1\theta}, R_2, R_{2\theta}, \ldots, R_{n-1}$, and $R_{(n-1)\theta}$.

(3) Substitute the known expressions for R_m into $h_{ln}(\theta)$, $m < n$ and use (58) to test whether (62) has a divergent solution. If $h_{ln[l]} \neq 0$, stop. This case cannot be finitely deformed.

(4) If the solution of (62) is not divergent, use (59)–(61) to generate R_{n+1} and repeat from step 2 with $n \to n+1$.

Appendix recalls some results on series expansions of derivatives and products of Legendre polynomials that are used in implementing these steps.

For a finite deformation, this algorithm would never terminate. However, in all cases that we have checked, we find a divergence at some order and so the horizon cannot be finitely deformed.

Explicitly, the first four even l cases are

$$\left.\frac{R}{m}\right|_{l=0} \approx 1 + P_0\epsilon + (\text{divergent term})\epsilon^2 \tag{63}$$

$$\left.\frac{R}{m}\right|_{l=2} \approx \frac{1}{4} + P_2\epsilon + (\text{divergent term})\epsilon^2 \tag{64}$$

$$\left.\frac{R}{m}\right|_{l=4} \approx \frac{1}{11} + P_4\epsilon + (\text{divergent term})\epsilon^2 \tag{65}$$

$$\left.\frac{R}{m}\right|_{l=6} \approx \frac{1}{22} + P_6\epsilon + (\text{divergent term})\epsilon^2, \tag{66}$$

while the first three odd cases are

$$\begin{aligned}\left.\frac{R}{m}\right|_{l=1} \approx{}& \frac{1}{2} + P_1\epsilon + 4\left(\frac{P_0 - P_2}{3}\right)\epsilon^2 + 16\left(\frac{-P_1 + P_3}{5}\right)\epsilon^3 \\ &+ 8\left(-\frac{17}{15}P_0 + \frac{7}{3}P_1 + \frac{1}{21}P_2 - \frac{131}{105}P_4\right)\epsilon^4 \\ &+ (\text{divergent term})\epsilon^5\end{aligned} \tag{67}$$

$$\begin{aligned}\left.\frac{R}{m}\right|_{l=3} \approx{}& \frac{1}{7} + P_3\epsilon + \left(-\frac{11}{12}P_0 + \frac{8}{9}P_2 + \frac{35}{2}P_3\right. \\ &\left. - \frac{351}{44}P_4 - \frac{940}{99}P_6\right)\epsilon^2 + (\text{divergent term})\epsilon^3\end{aligned} \tag{68}$$

$$\begin{aligned}\left.\frac{R}{m}\right|_{l=5} \approx{}& \frac{1}{16} + P_5\epsilon + \left(-\frac{1312}{165}P_0 - \frac{12200}{1287}P_2 - \frac{3456}{715}P_4\right. \\ &+ 112P_5 - \frac{41600}{1683}P_6 - \frac{190400}{8151}P_8 - \frac{9620856}{230945}P_{10}\left.\right)\epsilon^2 \\ &+ (\text{divergent term})\epsilon^3.\end{aligned} \tag{69}$$

In these expressions, the $\cos\theta$ dependence of the P_n is suppressed. The pattern appears to continue for all $l > 1$: that is even l diverge at second order while odd cases diverge at third order. This is demonstrated in Fig. 9, where $h_{l2[l]}$ and $h_{l3[l]}$ are plotted up to $l = 31$.

Though the trend in Fig. 9 seems clear, we were not able to show that the growth continues for all l: the expressions, particularly for the odd cases, become prohibitively complex.

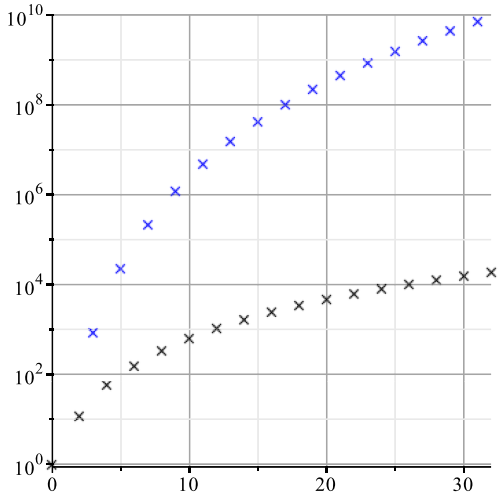

FIG. 9. $-h_{l2[l]}$ (black) and $h_{l3[l]}$ (blue) for even and odd cases, respectively, for $l = 2$ to $l = 31$. Both appear to be growing monotonically.

However, we can at least see why the odd cases do not diverge at second order. Reading off h_{2l} from (53) and keeping in mind that $R_{1l} = P_l(\cos\theta)$ then applying (A4), it is straightforward to see that on expanding the R_1^2 term into a Legendre series we only obtain even terms. Meanwhile, the $R_{1\theta}^2$ term can be expanded using (A1) and then (A4) again to see that it also contains only even terms. Hence, $h_{2l[l]}$ necessarily vanishes for all odd l, and any divergence must be at third or higher order.

V. DISCUSSION

While a stable MOTS cannot be smoothly deformed, "instability" is not sufficient to imply that such deformations are possible. For spherically symmetric MOTS in similarly symmetric spacetimes, we first showed that all but a few finely tuned cases are not deformable. Then on checking those special cases for RN spacetimes, we saw that, apart from pure de Sitter spacetime, none of them appeared to be deformable either (though we did not find a completely general proof).

Hence, we expect that a much stronger result holds that prevents (virtually all) horizons from being deformed. We expect that only spacetimes with extra symmetries (such as pure de Sitter) can house deformable MOTS, and that those deformations will turn out to be translations.

This would not be a particularly shocking result. It would be much more surprising to discover that inner black hole MOTS could be finitely deformed. However, as far as we know, there is no extant theorem that proves this.

ACKNOWLEDGMENTS

This work was supported by NSERC Discovery Grants No. 261429-2013 (I. B.) and No. 418537-2012 (H. K.). A. O. was also supported by an NSERC Undergraduate

Student Research Award and a Memorial University Student Internship Award.

APPENDIX: USEFUL LEGENDRE IDENTITIES

In this appendix, we recall how to expand the derivative and product of Legendre polynomials as a Legendre series. These are used in solving the horizon deformation equations.

1. Derivatives

By the standard recurrence relations, it is straightforward to show that the derivative of a Legendre polynomial can be expanded as

$$P_l'(\cos\theta) = \left\{ \begin{array}{ll} \sum_{m=1}^{l/2}(4m-1)P_{2m-1}(\cos\theta) & l \text{ even} \\ \sum_{m=0}^{(l-1)/2}(4m+1)P_{2m}(\cos\theta) & l \text{ odd} \end{array} \right\}, \tag{A1}$$

where $P_l'(x) = dP_l(x)/dx$.

2. Products

Next recall that the integral of three polynomials $P_k(x)$, $P_l(x)$, and $P_m(x)$ is given by the Wigner 3j symbol,

$$\int_{-1}^{1} P_k P_l P_m dx = 2\begin{pmatrix} k & l & m \\ 0 & 0 & 0 \end{pmatrix}^2, \tag{A2}$$

where if $|k-l| \le m \le k+l$ and $2s = m+k+l$ is even, then

$$\begin{pmatrix} k & l & m \\ 0 & 0 & 0 \end{pmatrix}^2 = \frac{(2s-2k)!(2s-2l)!(2s-2m)!}{(2s+1)!} \times \left(\frac{s!}{(s-k)!(s-l)!(s-m)!}\right)^2, \tag{A3}$$

else it is zero.

Then we can series expand the product of polynomials as a finite series,

$$P_k P_l = \sum_{m=|k-l|}^{k+l} (2m+1)\begin{pmatrix} k & l & m \\ 0 & 0 & 0 \end{pmatrix}^2 P_m. \tag{A4}$$

For purposes of the discussion in the main text, the important point is that for $k+l$ even, there are only even terms in the expansion, while for $k+l$ odd, there are only odd terms.

[1] S. A. Hayward, General laws of black hole dynamics, Phys. Rev. D **49**, 6467 (1994).
[2] A. Ashtekar and G. J. Galloway, Some uniqueness results for dynamical horizons, Adv. Theor. Math. Phys. **9**, 1 (2005).
[3] A. Ashtekar and B. Krishnan, Isolated and dynamical horizons and their applications, Living Rev. Relativity **7**, 10 (2004).
[4] I. Bengtsson and J. M. M. Senovilla, Region with trapped surfaces in spherical symmetry, its core, and their boundaries, Phys. Rev. D **83** (2011).
[5] R. Bousso and N. Engelhardt, New Area Law in General Relativity, Phys. Rev. Lett. **115**, 081301 (2015).
[6] R. P. A. C. Newman, Topology and stability of marginal 2-surfaces, Classical Quantum Gravity **4**, 277 (1987).
[7] L. Andersson, M. Mars, and W. Simon, Local Existence of Dynamical and Trapping Horizons, Phys. Rev. Lett. **95**, 111102 (2005).
[8] I. Booth and S. Fairhurst, Isolated, slowly evolving, and dynamical trapping horizons: Geometry and mechanics from surface deformations, Phys. Rev. D **75**, 084019 (2007).
[9] I. Booth, Black hole boundaries, Can. J. Phys. **83**, 1073 (2005).
[10] J. M. M. Senovilla, Classification of spacelike surfaces in spacetime, Classical Quantum Gravity **24**, 3091 (2007).
[11] S. A. Hayward, Involute, minimal, outer and increasingly trapped spheres, Phys. Rev. D **81**, 024037 (2010).
[12] K. Martel and E. Poisson, Regular coordinate systems for Schwarzschild and other spherical space-times, Am. J. Phys. **69**, 476 (2001).
[13] T. W. Baumgarte and S. L. Shapiro, *Numerical Relativity: Solving Einstein's Equations on the Computer* (Cambridge University Press, New York, New York, USA, 2010).
[14] J. Thornburg, Event and apparent horizon finders for 3 + 1 numerical relativity, Living Rev. Relativ. **10**, 3 (2007).
[15] Maple 2016. Maplesoft, a division of Waterloo Maple Inc., Waterloo, Ontario.